JACS
JOURNAL OF THE AMERICAN CHEMICAL SOCIETY

ARTICLE

pubs.acs.org/JACS

Structures and Dynamic Behavior of Large Polyhedral Coordination Cages: An Unusual Cage-to-Cage Interconversion

Andrew Stephenson,[†] Stephen P. Argent,[†] Thomas Riis-Johannessen,[‡] Ian S. Tidmarsh,[†] and Michael D. Ward*[,†]

[†]Department of Chemistry, University of Sheffield, Sheffield S3 7HF, United Kingdom

[‡]School of Chemistry, University of Bristol, Cantock's Close, Bristol BS8 1TS, United Kingdom

Supporting Information

ABSTRACT: The bis-bidentate bridging ligand L {α,α′-bis-[3-(2-pyridyl)pyrazol-1-yl]-1,4-dimethylbenzene}, which contains two chelating pyrazolyl-pyridine units connected to a 1,4-phenylene spacer via flexible methylene units, reacts with transition metal dications to form a range of polyhedral coordination cages based on a 2M:3 L ratio in which a metal ion occupies each vertex of a polyhedron, a bridging ligand lies along every edge, and all metal ions are octahedrally coordinated. Whereas the Ni(II) complex $[Ni_8L_{12}](BF_4)_{12}(SiF_6)_2$ is an octanuclear cubic cage of a type we have seen before, the Cu(II), Zn(II), and Cd(II) complexes form new structural types. $[Cu_6L_9](BF_4)_{12}$ is an unusual example of a trigonal prismatic cage, and both Zn(II) and Cd(II) form unprecedented hexadecanuclear cages $[M_{16}L_{24}]X_{32}$(X = ClO_4 or BF_4) whose core is a skewed tetracapped truncated tetrahedron. Both Cu_6L_9 and $M_{16}L_{24}$ cages are based on a cyclic helical M_3L_3 subunit that can be considered as a triangular "panel", with the cages being constructed by interconnection of these (homochiral) panels with additional bridging ligands in different ways. Whereas $[Cu_6L_9](BF_4)_{12}$ is stable in solution (by electrospray mass spectrometry, ES-MS) and is rapidly formed by combination of $Cu(BF_4)_2$ and L in the correct proportions in solution, the hexadecanuclear cage $[Cd_{16}L_{24}](BF_4)_{32}$ formed on crystallization slowly rearranges in solution over a period of several weeks to the trigonal prism $[Cd_6L_9](BF_4)_{12}$, which was unequivocally identified on the basis of its ^{1}H NMR spectrum. Similarly, combination of $Cd(BF_4)_2$ and L in a 2:3 ratio generates a mixture whose main component is the trigonal prism $[Cd_6L_9](BF_4)_{12}$. Thus the hexanuclear trigonal prism is the thermodynamic product arising from combination of Cd(II) and L in a 2:3 ratio in solution, and arises from both assembly of metal and ligand (minutes) and rearrangement of the Cd_{16} cage (weeks); the large cage $[Cd_{16}L_{24}](BF_4)_{32}$ is present as a minor component of a mixture of species in solution but crystallizes preferentially.

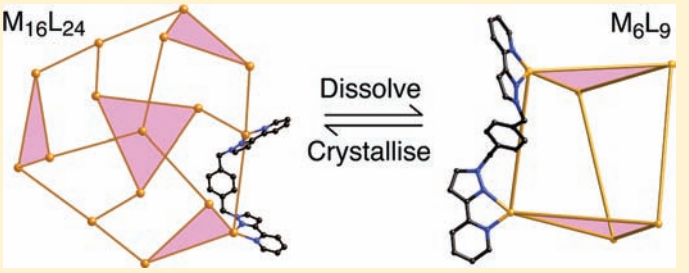

INTRODUCTION

Polyhedral coordination cages continue to attract attention because of their appeal in two distinct areas.[1−3] First, their formation by self-assembly from relatively simple components provides a test casefor our understanding of self-assembly and our ability to control it. As more examples are prepared and the geometric principles behind their formation become more apparent, rational design is playing an increasingly important role in the synthesis of new examples.[2d,3e] Second, the ability of some cages to act as hosts for a range of small molecules or ions,[3] and provide a constrained environment in which the reactivity of guest species is modified, has resulted in remarkable examples of cages being used as catalytic "microreactors".[3a,3b]

Our interest in this field has been based on the study of a family of cage complexes based on flexible bridging ligands in which two or three pyrazolyl-pyridine chelating units are connected to a central aromatic core via methylene groups.[1e] The flexibility of these ligands, afforded by free rotation of the chelating termini around the methylene spacers, is simultaneously essential and frustrating. It allows the assembly of ligands to adopt whatever conformations are needed to satisfy the coordination requirements of a particular array of metal ions, and thereby makes possible assembly of cages of remarkable complexity in which interligand interactions (and not just metal−ligand interactions) play an important role. However, this flexibility also precludes the possibility of rational design, which, so far, is based on rigid ligands with well-defined geometric properties.

In this contribution we show how a simple bis-bidentate bridging ligand L (see Chart 1 for structure) forms three different types of polyhedral cage when combined with different six-coordinate transition metal dications. These include two examples of $[M_{16}L_{24}]^{32+}$ cages—the largest members of this series yet characterized—which are based on a metal cage with a tetracapped truncated tetrahedral structure; a $[M_8L_{12}]^{16+}$ cage with a cubic core; and a $[M_6L_9]^{12+}$ cage that is unusual in being based

Received: August 17, 2010
Published: December 22, 2010

Chart 1. Structural Formula of the Bridging Ligand L and Two Related Ligands

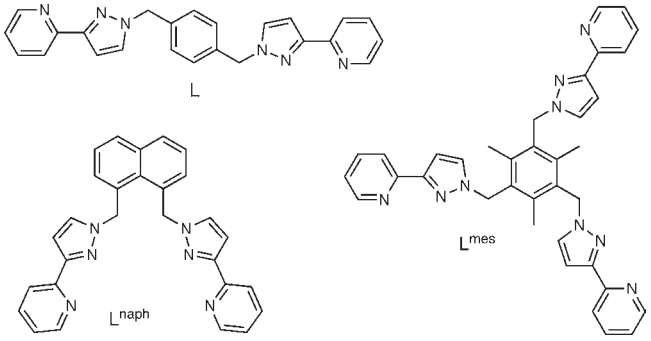

on a trigonal prismatic metal core. Solution studies reveal that there can be complicated dynamic behavior in solution with the largest $[M_{16}L_{24}]^{32+}$ cages formed on crystallization slowly converting to (principally) the $[M_6L_9]^{12+}$ trigonal prismatic cage in solution (see Table of Contents graphic).

One of the crystal structures in this paper has been briefly reported in a preliminary communication.[4]

RESULTS AND DISCUSSION

For our studies with this ligand we prepared complexes with Ni(II), Cu(II), Zn(II), and Cd(II) as their fluoroborate or perchlorate salts. Given the propensity of these ions to form six-coordinate tris-chelate geometries, and the bis-bidentate nature of the ligand L, we expect that whatever the structure of the assembly it will necessarily contain a 2:3 metal:ligand ratio based on simple stoichiometric considerations. This principle has been expressed in a range of cages such as M_4L_6 tetrahedra, M_8L_{12} cubes, and others.[1e]

1. Solid-State Structures. *Hexadecanuclear Cages with Zn(II) and Cd(II).* Reaction of L with $Zn(BF_4)_2$ or $Cd(ClO_4)_2$ in MeCN in a 3:2 ratio afforded a clear solution from which X-ray-quality crystals grew slowly following diffusion of diethyl ether vapor into the solution. X-ray analysis revealed formation of cages $[M_{16}L_{24}]X_{32}$ (M = Zn, X = BF_4; M = Cd, X = ClO_4), which are the largest members of this series of cages that we have identified so far.

The structure of the complex cation of $[Cd_{16}L_{24}](ClO_4)_{32}$ is shown in Figures 1 and 2. The complex crystallized in space group *P*-1, with no symmetry elements within the cage, such that every atom in an entire cage complex is crystallographically unique. The polyhedral core described by the metal ions as based on a M_{12} truncated tetrahedron[1g,5]—the simplest Archimedean solid, containing a mixture of triangular and hexagonal faces—but with (i) an additional metal ion capping each of the hexagonal faces and (ii) a distortion in which each of the four triangular faces is slightly twisted in the same sense, thereby removing the planes of symmetry of a basic truncated tetrahedron but retaining the four 3-fold rotation axes such that the polyhedral M_{16} core has (nonideal) *T* symmetry (Figure 1a). Conveniently, and following the stoichiometric requirements of having a M_2L_3 ratio, this M_{16} polyhedron has 24 edges; and one bridging ligand lies along each edge. Thus every bridging ligand spans two metal ions, and every metal ion at a vertex of the polyhedron—which lies at the conjunction of three edges—has a pseudo-octahedral tris-chelate coordination geometry arising from interaction with three different ligands.

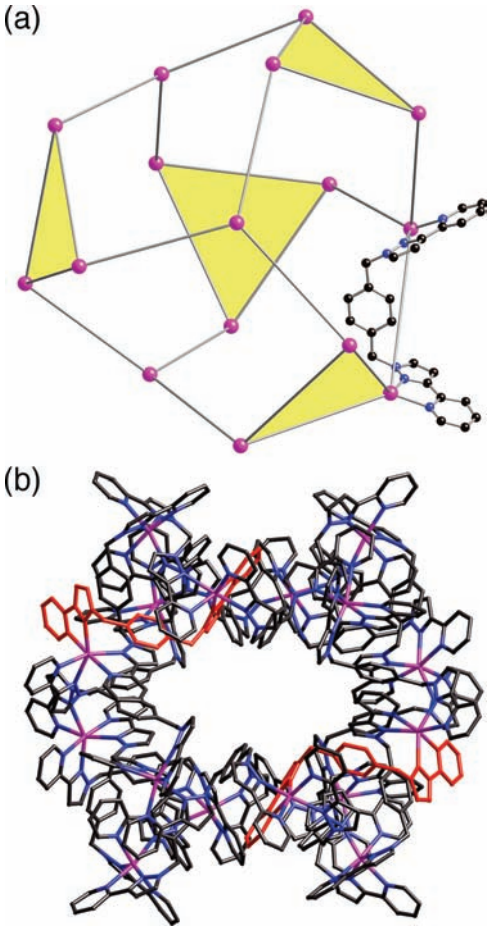

Figure 1. Two views of the structure of the complex cation of $[Cd_{16}(\mu\text{-}L)_{24}](ClO_4)_{32}\cdot 23MeCN$: (a) the capped truncated-tetrahedral core, with one edge-bridging ligand included (the faces colored yellow are those notionally derived from truncating the parent tetrahedron); (b) view showing all atoms in the cage, with two bridging ligands colored red (Cd, purple: N, blue).

Of the 16 metal centers, the 12 associated with the four triangular faces have meridional tris-chelate coordination environments arising from the nonsymmetrical (pyridine + pyrazole) chelating units. In contrast, the four capping metal centers have facial tris-chelate environments. Remarkably, all 16 tris-chelate metal centers have the same optical configuration in each cage complex, which appears to be necessary for a closed surface to form. The crystal is racemic, however. The Cd···Cd separations along the edges cover the range 9.04−10.17 Å, with the average value being 9.65 Å. The Cd···Cd separations around the triangular faces, connecting each pair of meridionally coordinated metal centers, average 9.81 Å, which is slightly longer than the average Cd···Cd separation between a cap and a triangular face (9.48 Å). Cd−N bond distances are in the range 2.28−2.45 Å.

One can imagine breaking this structure down into two components: a set of four M_3L_3 trinuclear cyclic helicates, with a vacant site for an additional bidentate ligand at each metal center; these are connected together via the capping ML_3 fragments, which, with three vacant chelating sites, act like a large triangular complex ligand (Figure 2). This way of looking at the structure—a set of interconnected triangular panels, each panel being a M_3L_3 cyclic helicate—is valuable, because it clarifies a common

dx.doi.org/10.1021/ja107403p |*J. Am. Chem. Soc.* 2011, 133, 858–870

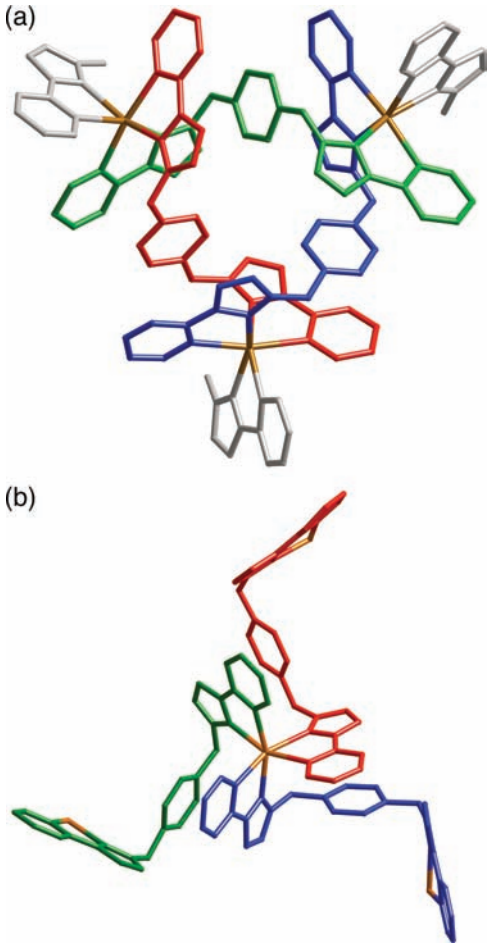

Figure 2. Decomposition of the crystal structure of the $[Cd_{16}(\mu\text{-}L)_{24}]^{32+}$ complex cation into its component parts. (a) One of the four $Cd_3(\mu\text{-}L)_3$ cyclic helical arrays with approximate C_3 symmetry, which constitute the triangular faces (shaded in Figure 1a); note the *meridional* tris-chelate arrangement at all metal centers and the additional ligand fragments (in gray) that connect to three different capping *fac*-CdL_3 units. (b) One of the four "capping" CdL_3 units that connect the $Cd_3(\mu\text{-}L)_3$ triangles; note the *facial* tris-chelate arrangement and the approximate C_3 symmetry.

structural principle that underpins several superficially quite different structures that we have described before, as well as another one later in this paper. We return to this point below.

The 24 bridging ligands spanning the edges of the polyhedron are intimately entangled with one another, with aromatic π-stacking between ligands being an important feature of the assembly. In particular, every central (electron-rich) phenylene spacer is sandwiched between pyrazolyl-pyridine units of two other ligands that are electron-deficient by virtue of coordination to a dipositive metal cation. This results in five-component ADADA (A = electron acceptor, D = electron donor) stacks like that shown in Figure 3, of which there are 12 around the periphery of the complex, thereby providing substantial enthalpic stabilization of the assembly.[6] The presence of 48 individual DA pairwise interactions in these stacks goes some way toward accounting for the formation of such a large structure, which is entropically disfavored compared to a larger number of smaller assemblies. We have shown in related work how this leads to a detectable interligand charge-transfer transition in some cases, which helps to stabilize the elaborate cage assemblies.[7]

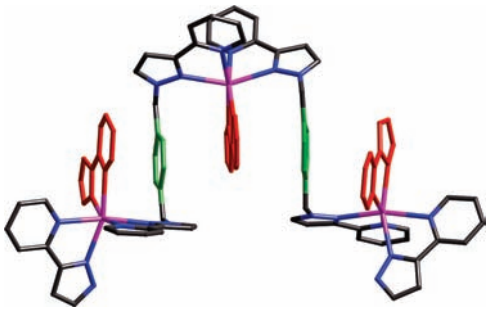

Figure 3. Five-layer aromatic stack in the structure of $[Cd_{16}(\mu\text{-}L)_{24}](ClO_4)_{32}$ with electron-rich (phenyl) rings in green and electron-deficient (pyrazolyl-pyridine) units in red.

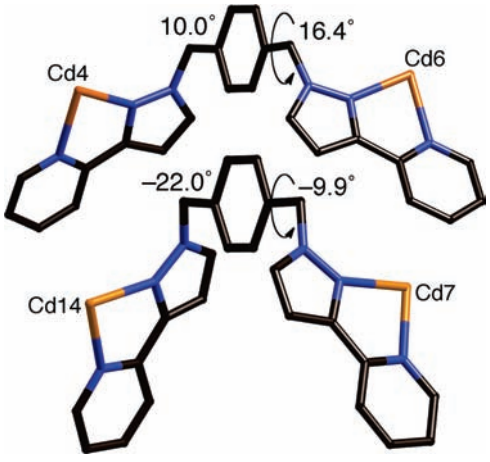

Figure 4. Conformations of some of the bridging ligands in the structure of $[Cd_{16}(\mu\text{-}L)_{24}](ClO_4)_{32}$.

Given the range of possible conformations that these flexible ligands could adopt, all of the ligands in the cage show a surprising degree of conformational similarity. The two pyrazolyl-pyridine units are directed toward the same edge of the central phenylene group such that each ligand L has an overall U shape rather than an S shape; the chelating pockets, however, are oriented toward opposite faces of the phenylene groups, coming out of and into the page in the view shown in Figure 4. The C(phenyl)−C(methylene)−N(pyrazolyl)−N(pyrazolyl) torsion angles are close to 90° such that the planes of the pyrazolyl-pyridine groups are twisted as far as possible away from the plane of the phenylene group. This arrangement gives each ligand approximate (noncrystallographic) C_2 symmetry with the axis lying in the plane of, and bisecting, the central phenylene ring. The range of differing Cd···Cd separations is accommodated by variations in the torsion angle about the C(phenylene)−C(methylene) bonds as shown in Figure 4, which shows the bridging ligand spanning the shortest metal−metal edge [Cd(7)−Cd(14), 9.04 Å] and the longest [Cd(4)−Cd(6), 10.17 Å].

The size of the central cavity can be estimated from the shortest H···H contacts across the middle, which are ca. 13 Å. Allowing for the van der Waals radii of the H atoms gives an effective void diameter of 11 Å, or a volume of ca. 700 $Å^3$. In the crystal this cavity contains (at least) eight anions and six MeCN molecules; this cavity is very open given the large access channels through the centers of the faces of the polyhedron (Figure 1b).

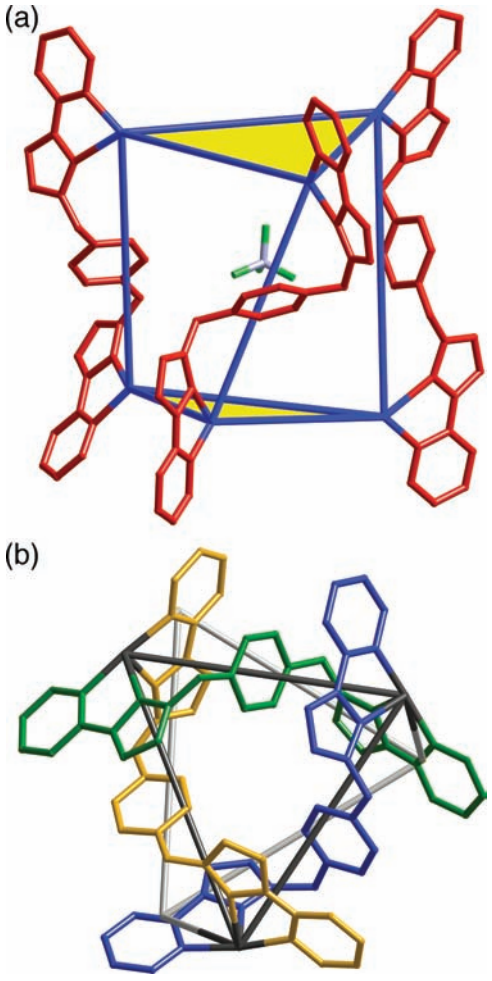

Figure 5. Two views of the trigonal prismatic complex cation of $[Cu_6L_9](BF_4)_{12}$: (a) view showing the three "pillar" ligands that connect the two triangular faces and (b) view emphasizing the twist between the two triangular faces, which are slightly offset.

$[Zn_{16}L_{24}](BF_4)_{32}$ was also structurally characterized and is isostructural with the Cd(II) complex; it crystallizes in space group *C*2/*c*, astride a *C*2 axis such that only half of the complex is crystallographically unique in this case. Despite the lower ionic radius of Zn(II) compared to Cd(II), and the resultant shorter M−N bond distances (in the range 2.08−2.30 Å), the structure is essentially identical to that of $[Cd_{16}L_{24}](ClO_4)_{32}$. The Zn···Zn separations along the edges of the polyhedral cage average 10.33 Å around the triangular helical faces and 9.42 Å along the edges that connect a triangular face to a cap, giving an overall average of 9.87 Å, slightly *longer* that in the Cd_{16} cage. All other features of the complex are comparable to those of the Cd_{16} complex.

Trigonal Prismatic Hexanuclear Cage with Cu(II). The same synthetic procedure, combining L with Cu(II) salts in a 3:2 ratio followed by slow crystallization, afforded crystals of what proved to be the hexanuclear cage $[Cu_6L_9](BF_4)_{12}$ (Figures 5 and 6). This cage has an approximately trigonal prismatic topology, with Cu(1), Cu(2), and Cu(3) forming one triangular face and Cu(4), Cu(5), and Cu(6) the other. The presence of a bridging ligand along every one of the nine edges affords the 2:3 metal:ligand ratio that is required for all metal centers to be six-coordinate. The two triangular faces are not exactly eclipsed but are offset

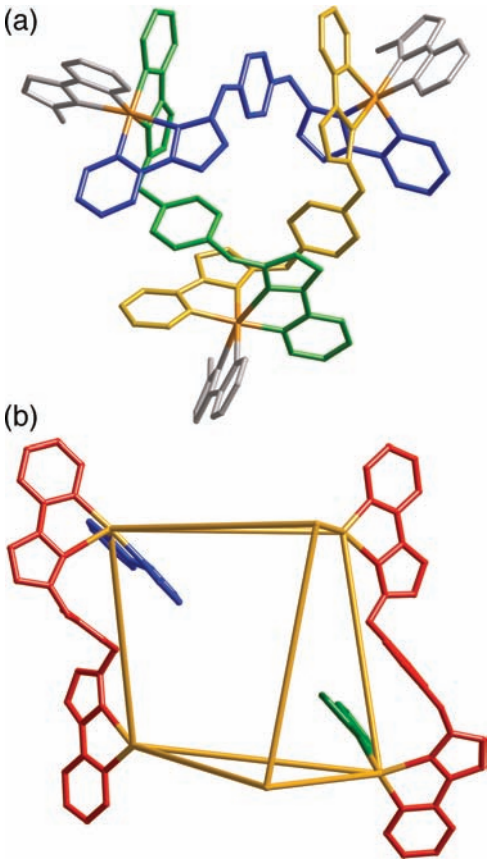

Figure 6. (a) One of the trinuclear helical fragments in the structure of $[Cu_6L_9](BF_4)_{12}$ (cf. Figure 2a); (b) interligand aromatic stacking between the pillaring ligands (in red) and fragments of ligands around the triangular faces (shown in blue and green).

such that the basic core structure is distorted toward a trigonal antiprism (Figure 5b).

Although this is quite a different structure from the M_{16} cages reported above, it does have an important similarity in that it contains two Cu_3L_3 cyclic helical faces, which are homochiral such that all six metal centers have the same optical tris-chelate configuration. Relaxation of this structure in solution would therefore result in D_3 symmetry, with a C_3 axis through the center of, and perpendicular to, the two triangular faces; and three C_2 axes perpendicular to this, each one bisecting one of the "pillar" ligands and projecting through the opposite rectangular face, allowing the top and bottom (homochiral) triangular faces to interconvert. We will return to this point later.

As before, the Cu_3L_3 cyclic helical units are based on meridional tris-chelate centers with the three ligands arranged in a ring such that the central phenylene spacer of one is sandwiched between the coordinated pyrazolyl-pyridine units of the other two. The M_3L_3 units from the two structures are very similar (compare Figures 2a and 6a). The difference in the structures of the $M_{16}L_{24}$ and M_6L_9 cages arises from the fact that, in the former case, four of these are connected by triply bridging *fac*-ML_3 units; but in the latter case only two M_3L_3 units are connected by three bridging ligands acting as pillars (the ligands shown in red in Figure 5a), which is the simplest way that two such triangular units could be connected together. The Cu···Cu separations average 10.20 Å around the two triangular faces and 10.56 Å for

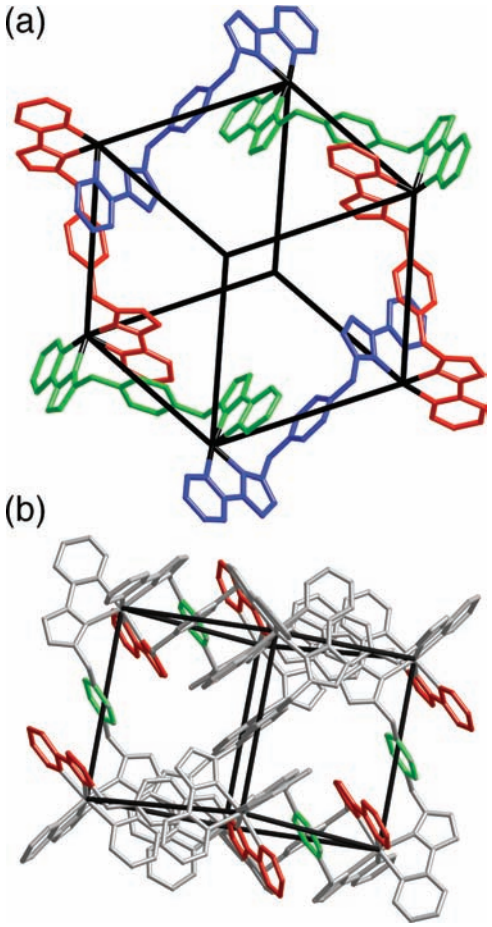

Figure 7. Two views of the octanuclear cubic cation of $[Ni_8L_{12}](BF_4)_{12}(SiF_6)_2$: (a) disposition of metal ions and the arrangement of some of the edge-bridging ligands; (b) view of the complete cage emphasizing two of the five-component aromatic stacks with electron donor and acceptor components colored in green and red, respectively (cf. Figure 3).

the other three edges between the triangular faces; the overall average Cu···Cu separation is 10.32 Å.

Compared to the M_{16} cages, $[Cu_6L_9](BF_4)_{12}$ shows more irregular metal coordination (because of the Jahn−Teller effect associated with Cu(II)] and also greater variation in the conformations adopted by the bridging ligands. The Cu−N distances vary from 1.95 to 2.45 Å, with every metal center having one axis—in each case, the axis with two pyrazole ligands—being substantially elongated compared to the other two. The six ligands around the two triangular faces have the same U-shaped conformation as those seen in the M_{16} cages, with minor variations (see Figure 4). In contrast the three ligands that connect the two triangular faces are more S-shaped in their conformations, with the two pyridyl-pyrazole units directed to opposite sides of the central phenylene spacer; this is apparent in Figure 5a. These conformations allow the central phenylene groups of these three pillar ligands also to participate in π-stacking with pyridyl-pyrazole units around the triangular faces, which is shown in Figure 6b.

The central cavity of the cage contains a $[BF_4]^-$ anion that is anchored by a network of CH···F hydrogen-bonding interactions (with C···F distances in the range 2.89−3.37 Å) from inward-pointing CH protons of pyrazole and methylene groups.

Identification of a trigonal prismatic cage in this series is welcome as it fills an obvious gap. The requirement for a 2:3 metal:ligand stiochometry, with a metal at each vertex and a bridging ligand along each edge,[1e] is met by a limited number of polyhedra of which the M_4L_6 tetrahedron, M_6L_9 trigonal prism, and M_8L_{12} cube are the simplest examples. We have identified many examples of both M_4L_6 tetrahedra[8] and M_8L_{12} cubes[7,9] based on this family of ligands, and interestingly both of those are platonic solids. The platonic polyhedron containing six vertices is an octahedron, but that has 12 edges, giving a vertex:edge ratio of 1:2 rather than 2:3, and therefore cannot be formed solely from octahedral metal centers at the vertices (three-connected) and edge-bridging ligands (two-connected). Of course a trigonal prismatic arrangement of bulky groups is inherently less stable than an octahedral arrangement because the two triangular faces are eclipsed rather than staggered, increasing steric repulsions between them. Consequently trigonal prismatic cage structures are relatively rare and are often based on rigid triangular ligands that provide the top and bottom faces of the assembly and thereby impose 3-fold symmetry (cf. examples from Stang and co-workers,[10] Kaim and co-workers,[11] and Ghosh and Mukherjee[12]). The closest related example to ours—with a metal ion at each vertex and a bridging ligand along each edge—appears to be $[\{Mo(CO)_3\}_6(\mu\text{-}CN)_9]^{9-}$ described by Contakes and Rauchfuss.[13]

Octanuclear Cubic Cage with Ni(II). In contrast to the above two structural types, reaction of L with $Ni(BF_4)_2$ in a 3:2 ratio in the same way afforded crystals of what proved to be the octanuclear cage $[Ni_8L_{12}](BF_4)_{12}(SiF_6)_2$ (with the hexafluorosilicate presumably arising from hydrolysis of tetrafluoroborate in a glass vial during slow crystallization, and these crystals therefore not being representative of the bulk, which analyzed satisfactorily as $[Ni_8L_{12}](BF_4)_{16}$). This is illustrated in Figure 7 and has the same basic structure as several other types of cubic cage we have reported recently[7,9], so a detailed description of the structure is not required. The main features of the structure may be summarized as follows. (i) The eight Ni(II) ions are arrayed at the corners of a slanted cube, with Ni···Ni separations along the edges of 10.20 Å [Ni(2)···Ni(1)] and 10.57 Å [Ni(1) to its symmetry equivalent], and there is a bridging ligand along each of the 12 edges of the cube; (ii) a diagonally opposite pair of Ni(II) ions [Ni(2) and its symmetry equivalent Ni(2A)] have a *fac*-tris-chelate geometry, whereas the other six ions [Ni(1) and its five symmetry equivalents] have *mer*-tris-chelate geometry; (iii) the assembly has S_6 symmetry with the Ni(2)···Ni(2A) axis constituting the coincident C_3 and S_6 axes; (iv) there is extensive interligand aromatic stacking with every central phenyl ring (relatively electron-rich) sandwiched between a pair of coordinated pyrazolyl-pyridine units (relatively electron-deficient), giving a total of eight five-layer alternating acceptor/donor/acceptor/donor/acceptor stacks, one associated with each face of the cube (Figure 7b); and (v) the central cavity contains a (disordered) fluoroborate anion.

Although this M_8L_{12} cube is a known structural type with other ligands,[7,9] its appearance here is interesting as we have observed three completely different types of solid-state structure in the cages formed by Ni(II), Cu(II), and Zn(II), all of which are six-coordinate tris-chelates. We ascribe this to differences in ionic radius and stereoelectronic preference. While Ni(II) and Zn(II) both form fairly regular six coordinate geometries, the Ni−N distances (all in the range 2.09−2.12 Å) are considerably less on average than the Zn−N distances (2.08−2.30 Å) because of the smaller ionic radius of Ni(II) compared to Zn(II) in octahedral

dx.doi.org/10.1021/ja107403p |*J. Am. Chem. Soc.* 2011, 133, 858–870

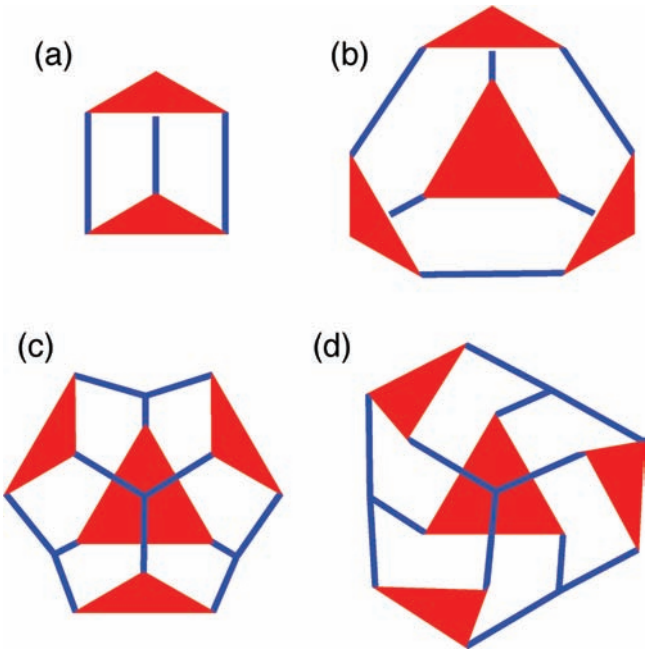

Figure 8. Schematic diagram showing how triangular M_3L_3 cyclic helicate units (shown as red panels) can be combined into a range of polyhedral cages. (a) Three bis-bidentate edge-bridging ligands combine two triangular panels into a trigonal prism (this work). (b) Four triangular panels can be combined via six edge-bridging ligands into a truncated tetrahedral array (ref 5a). (c) Four triangular panels can be combined via four tris-bidentate ligands L^{mes} into a cuboctahedral array (ref 2f). (d) Four triangular panels can be connected by a tris-bidentate unit consisting of a *fac*-ML_3 complex unit with three pendant bidentate binding sites (cf. Figure 2b, this work).

geometry. Cu(II) is of course a special case because of the Jahn−Teller effect, which leads to considerably more eccentric six-coordinate geometries than observed with either Ni(II) or Zn(II). On this basis it is not surprising that the Cd(II) cage is isostructural with the Zn(II) cage, as Cd(II) likewise has rather long M−N bonds but has no stereoelectronic preference for an irregular coordination geometry.

Some Underlying Similarities between Different Cages Based on Polyhedra with Triangular Faces. It is appropriate at this point to draw attention to a structural principle that appears to be the basis of many of the cages that we have observed, both in this work and from earlier work. It was mentioned earlier that both the $M_{16}L_{24}$ and M_6L_9 cages are based on triangular M_3L_3 cyclic helicate units, in which each metal center of the M_3L_3 fragment has one connection point for an additional pyrazolyl-pyridine unit to facilitate connection of these M_3L_3 fragments together, and every metal ion has a *mer*-tris-chelate geometry. In the case of the M_6L_9 trigonal prism, two such M_3L_3 fragments are connected to each other by three additional bridging ligands that act as pillars between the triangular panels, which is the simplest way in which two M_3L_3 fragments can be combined via ditopic ligands.

In the $M_{16}L_{24}$ cages, in contrast, there are four M_3L_3 fragments that are connected by four *fac*-ML_3 units, each of which acts as a triply bridging `complex ligand' with three pendant bidentate binding sites. Thus each *fac*-ML_3 unit connects to one vertex of three separate M_3L_3 units, and each M_3L_3 unit is likewise connected to three separate *fac*-ML_3 units. This is illustrated schematically in Figure 8 and reveals the underlying tetrahedral rotational symmetry (point group *T*): just as a tetrahedron has four vertices and four vertices, the $M_{16}L_{24}$ cage is formally related to this by having four M_3L_3 fragments (one located at each vertex of a tetrahedron) and four *fac*-ML_3 fragments (one lying over each of the four faces of the notional tetrahedron).

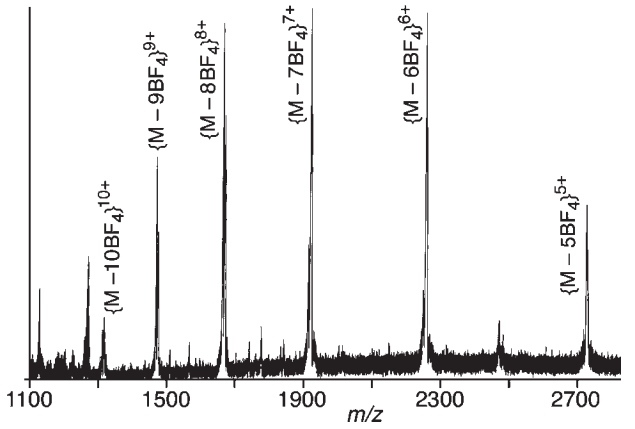

Figure 9. ES mass spectrum of redissolved crystals of $[Cd_{16}(\mu\text{-}L)_{24}](BF_4)_{32}$, showing the sequence of peaks corresponding to the intact cage with loss of varying numbers of counterions.

The relationship between the $M_{16}L_{24}$ cages and the previously reported mixed-ligand cuboctahedral cages $[M_{12}(\mu\text{-}L)_{12}(L^{mes})_4]^{24+}$ is clear. These cuboctahedral cages were the sole products formed when Cu(II) or Cd(II) salts were combined with a mixture of (edge-bridging) L and the triangular tris-chelating ligand L^{mes} (see Chart 1 for structure) in the correct proportions (Figure 8c).[2f] In this case, four cyclic trinuclear helicates M_3L_3 are held together in a *T*-symmetric array by four ligands L^{mes}, each of which donates one bidentate arm to a different M_3L_3 unit. Thus, the three-armed face-capping ligand L^{mes} fulfils precisely the same role in the cuboctahedral cages[2f] as do the *fac*-ML_3 units in the $M_{16}L_{24}$ cages (this work).

Finally we note that the previously reported truncated tetrahedral cages $[M_{12}(L^{naph})_{18}]X_{24}$ also fit into this series.[5a] These are based on a different bridging ligand, L^{naph} (see Chart 1), having a 1,8-naphthyl group as the core rather than 1,4-phenylene, but the principle is identical. These cages also contain four $M_3(L^{naph})_3$ triangular helical faces with *mer*-tris-chelate geometries. Instead of being connected by triply bridging fragments, however, as in the previous two examples, they are connected by additional linear bridging ligands L^{naph} such that each additional L^{naph} ligand connects a vacant coordination site from two triangular faces. Connection of four $M_3(L^{naph})_3$ triangles in this way requires an additional six L^{naph} ligands to give the observed structures.

These interesting similarities between quite disparate cage structures suggest a design principle that may provide the basis for (partly) rational assembly of new members of this series of cages by use of preassembled M_3L_3 units connected in different ways.

2. Solution Behavior. *Characterization by ES-MS and NMR Spectroscopy.* Solution characterization of $[Cd_{16}L_{24}](BF_4)_{32}$ confirmed satisfactorily that the complex retains its structure in solution (note: we used the perchlorate salt for the crystallographic study, as it scattered X-rays better, but used the fluoroborate salt—confirmed to be isostructural by crystallography—for subsequent spectroscopic studies). The ES mass spectrum showed a clear sequence of peaks for the series $\{Cd_{16}L_{24}(BF_4)_{32-n}\}^{n+}$ corresponding to sequential loss of perchlorate

dx.doi.org/10.1021/ja107403p |*J. Am. Chem. Soc.* 2011, 133, 858–870

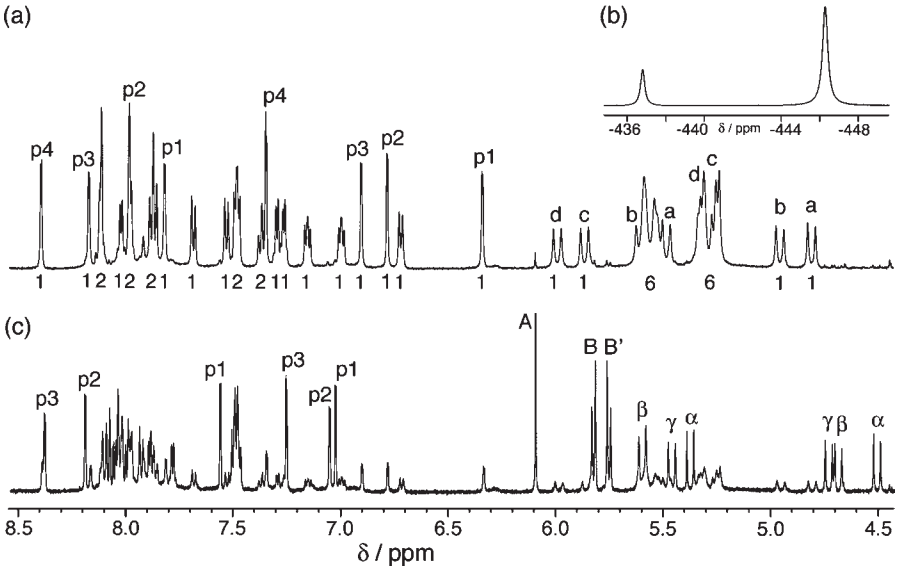

Figure 10. (a) Complete ^{1}H NMR spectrum of $[Cd_{16}(\mu\text{-L})_{24}](BF_4)_{32}$ in CD_3CN, measured immediately after dissolution of the crystals. The four pairs of diastereotopic CH_2 protons assosicted with two independent, nonsymmetric ligand environments are labeled a−d; likewise, the four pairs of pyrazolyl H^4/H^5 protons for four independent pyrazolyl rings are labeled p1−p4 (see text). (b) ^{113}Cd NMR spectrum of $[Cd_{16}(\mu\text{-L})_{24}](BF_4)_{32}$ in CD_3CN, measured immediately after dissolution of the crystals, showing the two Cd environments of the Cd_{16} cage in a 3:1 ratio. (c) Same sample as for spectrum a but measured 27 days later, showing near-complete conversion to $[Cd_6(\mu\text{-L})_9](BF_4)_{12}$. The labels α, β, and γ denote the three independent pairs of diastereotopic CH_2 protons; labels p1−p3 denote the three pairs of pyrazolyl H^4/H^5 protons; signals labeled A, B, and B′ relate to the phenyl protons associated with the symmetric and nonsymmetric ligand environments as shown in Figure 12.

anions from the intact complex core (Figure 9). The 500 MHz ^{1}H NMR spectrum revealed signals consistent with the presence of a total of 40 different proton environments of equal abundance, indicating the presence of two ligand environments (Figure 10a). There are 12 ligands associated with the triangular faces, each spanning two meridional metal centers, with the chirality of the complex ensuring that the two termini of each ligand (and hence all protons in each ligand) are inequivalent. In addition, there are another 12 ligands connecting the capping metal ions to the triangular faces, spanning one facial and one meridional metal center, whose termini are also necessarily inequivalent. Since each ligand has 20 protons, this generates the necessary 40 environments. Further confirmation comes from a COSY spectrum, which allows identification of the coupled pairs of protons associated with the methylene spacers: in a chiral environment the two protons of each -CH_2- group are diastereotopic, giving eight signals—doublets with characteristically large coupling constants—in four coupled pairs, which are labeled in Figure 10a. For exactly the same reasons there are four different types of pyrazolyl ring environment leading to eight doublets (four coupled pairs of signals) associated with the pyrazolyl rings; these are also labeled in Figure 10a. Finally, the 16 Cd(II) ions may be split into a set of 12 (meridional, around the triangular faces) and a set of four (facial, at the capping positions), and the ^{113}Cd NMR spectrum shows two signals in a 3:1 ratio, at chemical shifts of −446.3 and −436.8 ppm respectively, consistent with this (Figure 10b).

This Cd_{16} cage is therefore stable in solution, at least on a time scale of a few hours. Redissolved crystals of $[Zn_{16}L_{24}](BF_4)_{32}$, however, although they showed the expected series of peaks in the ES mass spectrum analogous to those in Figure 9, gave a messy and poorly resolved ^{1}H NMR spectrum containing far more than 40 signals. Thus the isostructural Zn_{16} complex undergoes dissociation or rearrangement of this complex following dissolution; this is discussed in more detail later.

The ES mass spectrum of redissolved crystals of $[Cu_6L_9](BF_4)_{12}$ likewise confirmed the integrity of the complex in solution, with a sequence of peaks at m/z 2391, 1565, 1152, and 904 corresponding to $\{Cu_6L_9(BF_4)_{12-n}\}^{n+}$ (n = 2−5) being observed with the correct fractional isotopic spacings according to the charges for each species. We could not identify any other peaks at high m/z characteristic of other cages, indicating not only that $[Cu_6L_9](BF_4)_{12}$ is intact in solution but also that it does not rearrange significantly to other cage types (see below). This spectrum did not change significantly with time.

The ESMS of $[Ni_8L_{12}](BF_4)_{12}(SiF_6)_2$ in solution was not so clear-cut, however. It showed at high m/z values some weak peaks corresponding to the intact cube $\{Ni_8L_{12}(BF_4)_{16-n}\}^{n+}$ (n = 2, at m/z 2376; n = 3, at m/z 2102) but also a series of more intense peaks corresponding to the hexanuclear complex $\{Ni_6L_9(BF_4)_{12-n}\}^{n+}$ at m/z 2376, 1554, and 1144 (n = 2−4), which we assume to arise from a trigonal prismatic cage. The assignment of these peaks was confirmed in every case by the isotopic spacings, which removes any ambiguity: for example, the peak at m/z 1554 can be definitely ascribed to $\{Ni_6L_9(BF_4)_9\}^{3+}$ and not $\{Ni_8L_{12}(BF_4)_{12}\}^{4+}$ because the successive peaks in the isotope cluster are one-third of a mass unit apart. The implication is that a mixture of a Ni_6 species (probably a trigonal prismatic cage) and a Ni_8 cubic cage forms in solution, but the Ni_8 cubic cage crystallizes preferentially.

The Ni_6 cage could therefore arise from rearrangement of the Ni_8 cube when it is dissolved, but in the absence of ^{1}H NMR data we cannot rule out the possibility that some of the Ni_6 species also forms in the solid state but does not crystallize. We have observed such a disparity between solid-state and solution structures in other examples of polynuclear cages.[9]

dx.doi.org/10.1021/ja107403p |J. Am. Chem. Soc. 2011, 133, 858–870

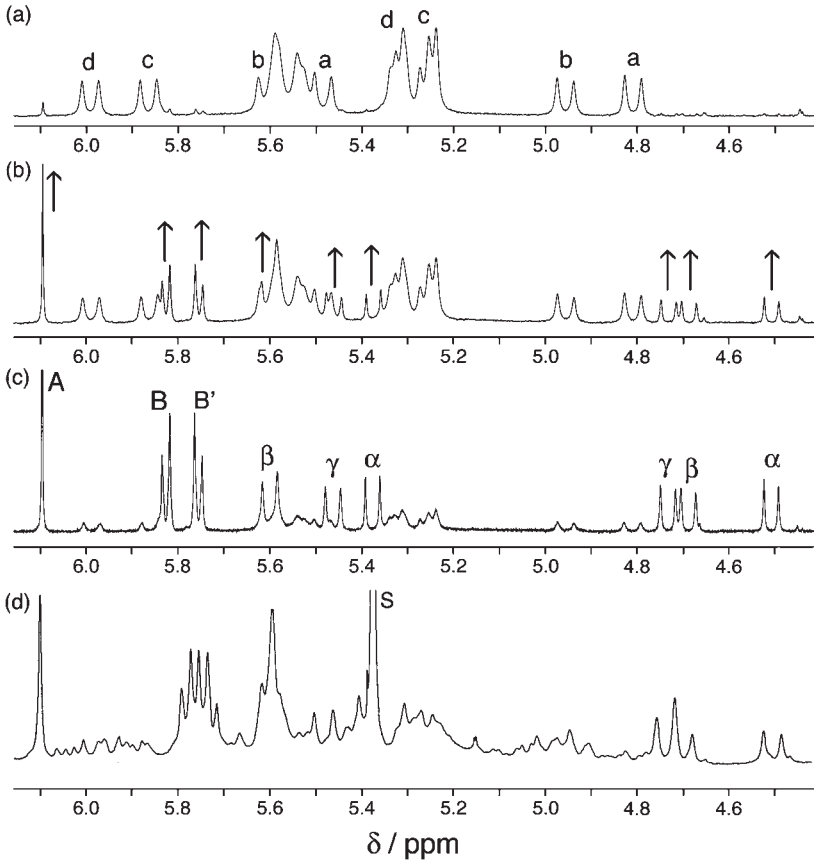

Figure 11. (a–c) Partial ^{1}H NMR spectra of $[Cd_{16}(\mu\text{-L})_{24}](BF_4)_{32}$ in CD_3CN taken at different times after sample preparation. (a) Spectrum immediately after dissolution: this is an expansion of Figure 10a. (b) Spectrum recorded 5 days after dissolution of the crystals, showing the grow-in of a new set of signals denoted by the arrows. (c) Spectrum recorded 27 days after dissolution: this is an expansion of Figure 10c. (d) Partial ^{1}H NMR spectrum of a CD_3CN solution containing a 2:3 mixture of $Cd(BF_4)_2$ and L, taken 30 min after mixing. The correspondence of the main features of this spectrum following assembly of the components with the main features of the spectrum of the Cd_6L_9 cage (panel c, immediately above) is obvious (see text). S = residual solvent.

Rearrangement of $[Cd_{16}L_{24}](BF_4)_{32}$ in Solution. As mentioned above, the ^{1}H and ^{113}Cd NMR spectra, and the ES mass spectrum, of the 16-nuclear cage $[Cd_{16}L_{24}](BF_4)_{32}$ were in agreement with the solid-state structure being retained on the time scale of the measurements. However, we observed that the same sample, left in solution, showed major changes in its ^{1}H NMR spectrum (Figure 11), which occurred over a period of a few weeks at room temperature. The series of peaks corresponding to $[Cd_{16}L_{24}](BF_4)_{32}$ slowly diminished in intensity and was replaced by a single new set of peaks corresponding to formation of one new species. The conversion appeared to be clean, with all new peaks growing in at the same rate, and took about two months until no further changes occurred, after which the ratio between new and old signals was ca. 10:1 on the basis of integration of signals. Thus the two components are in slow equilibrium. There is substantial overlap between the two sets of signals, with some signals hardly shifting between starting material and product, so complete deconvolution of the spectrum into two sets is not possible. However in the 4.5–6 ppm region where the methylene protons appear, it is clear that as the eight signals of the starting complex (four coupled pairs for four inequivalent diastereotopic CH_2 groups, as labeled in Figure 11a) disappear, they are replaced by another set of *six* signals, all of the same intensity, which likewise consist of three coupled pairs (on the basis of a COSY spectrum); see Figure 11b,c. Also appearing in this region are a singlet at 6.1 ppm and a coupled pair of doublets between 5.8 and 5.9 ppm, all associated with the product; these three signals have the same intensity as each other and twice the intensity of the doublets from the methylene protons.

This information is sufficient to allow us to identify the new product, as there is only one type of cage structure that we have observed that could give such a ^{1}H NMR spectrum, and that is a D_3-symmetric Cd_6L_9 trigonal prism, similar to the crystal structure we described above but with the highest possible symmetry due to relaxation in solution. This structure has two ligand environments: the six equivalent ligands around the two triangular helical faces, and the three equivalent ligands acting as the pillars between these triangular panels (see sketch in Figure 12). The six ligands around the triangular helical faces have no internal symmetry—the front and back ends of each ligand are inequivalent because of the chirality—but are all equivalent to one another. This gives two independent CH_2 groups affording four proton signals, each a doublet, and each with an intensity of 6H. The three pillar ligands, however, have 2-fold symmetry, as they will lie on C_2 axes (assuming that the cage has D_3 symmetry with the 3-fold axis through the two triangular faces). Thus there is only one additional CH_2 environment arising from the six equivalent halves of these three ligands. This will afford two more CH doublets, each with 6H intensity. The result is six methylene

dx.doi.org/10.1021/ja107403p |*J. Am. Chem. Soc.* 2011, 133, 858–870

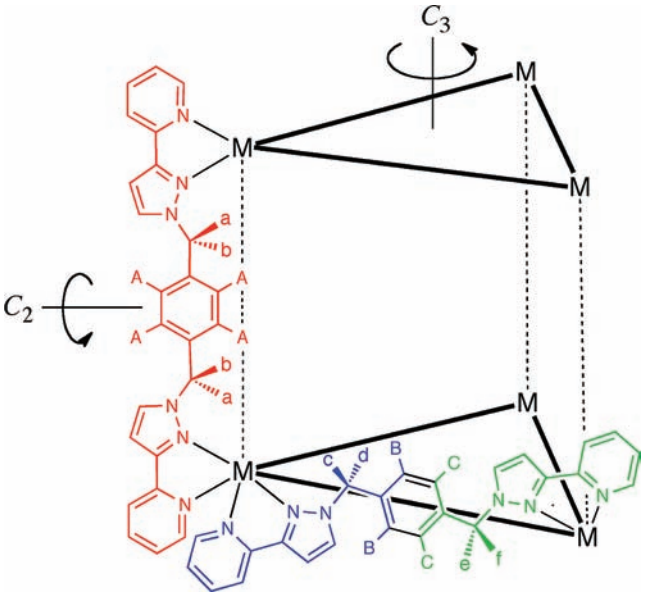

Figure 12. Sketch of a trigonal prismatic $[M_6(\mu\text{-L})_9]^{12+}$ complex cation, clarifying the evolution of NMR spectra shown in Figure 11. The two M_3 triangular faces (bold M−M lines) are cyclic trinuclear helicates (cf. Figure 6a), within which each ligand has two magnetically inequivalent termini due to the chirality (shown as blue and green ligand halves). These two triangles are connected by the red pillar ligands (cf. Figure 8a), which each have 2-fold symmetry such that both termini are equivalent. The result is three environments for each CH_2-pyrazolyl-pyridine group, with equal population of each, giving three pairs of methylene protons; and two environments for the central phenyl ring, of which the symmetric one gives a single signal and the other gives two doublets, exactly in agreement with the ^{1}H NMR spectra in Figures 10c and 11c.

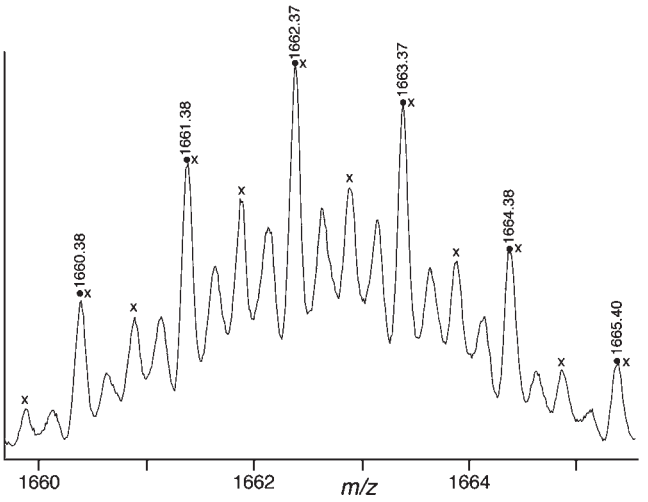

Figure 13. Part of the ES mass spectrum of redissolved crystals of $[Cd_{16}(\mu\text{-L})_{24}](BF_4)_{32}$ in CH_3CN 2 weeks after dissolution, showing a superposition of peak cluster with isotope spacings of 1 unit (labeled •), 0.5 unit (labeled ×), and 0.25 unit (all peaks), corresponding to a mixture of fragments $\{Cd_2L_3(BF_4)_3\}^+$, $\{Cd_4L_6(BF_4)_6\}^{2+}$, and $\{Cd_8L_{12}(BF_4)_{12}\}^{4+}$, which all have the same m/z value.

protons of equal intensity, as observed, arising from 1.5 independent ligand environments.

This would also require three independent environments for the pyrazolyl rings, and indeed three coupled pairs of protons for these can be observed in the full ^{1}H NMR spectrum shown in Figure 10b. The assignment is further supported by the three signals at 5.8, 5.9, and 6.1 ppm (Figure 11c), which correspond to the protons of the central phenylene spacers in the trigonal prismatic structure. The ligands around the triangular faces give the coupled pair of (second-order) doublets because the two protons near the head end of each ligand are different from the two protons near the tail end, affording an AB pattern with each component integrating to 12H. In contrast in the three pillar ligands, with 2-fold symmetry, the four phenylene protons are all equivalent in solution, giving a singlet corresponding to 12H (see Figure 12). As required, these three signals all have the same intensity and are double the intensity of each of the six methylene doublets (which integrate to 6H each).

The final piece of support for this structural rearrangement is provided by measurements of the diffusion coefficient of the starting Cd_{16} cage and the product, which were obtained from selected proton signals at a stage in the rearrangement when both sets of protons were of comparable intensity. On the basis of several independent measurements using separate well-isolated signals for the starting material ($Cd_{16}L_{24}$ cage) and product (Cd_6L_9 cage), diffusion coefficients of 3.74×10^{-10} and 5.21×10^{-10} $m^2 \cdot s^{-1}$, respectively, were obtained; putting these values into the Stokes−Einstein equation gives a molecular weight ratio of $(5.21/3.74)^3$, or 2.7:1, between starting material and product, assuming that the two species are approximately spherical. This agrees very well with the required 16:6 ratio (2.667:1).[14]

Significantly, no other cage that we have observed could give a ^{1}H NMR spectrum of the type we observe for the rearranged product, with six equal-intensity methylene proton signals indicative of 1.5 independent ligand environments. The M_8L_{12} cubes have two independent ligand environments, which would give eight methylene signals; M_4L_6 tetrahedral cages would give either two[15] or eight[16] methylene protons depending on whether they had T symmetry[15] or C_3 symmetry.[16] Warming the sample in the NMR tube accelerated the reaction substantially: a sample of the Cd_{16} complex kept at 60 °C showed an identical evolution of its ^{1}H NMR spectrum, with 90% conversion to the Cd_6 complex after 2 days.[17]

The ES mass spectrum of the same solution after rearrangement (2 months after the crystals of $[Cd_{16}L_{24}](BF_4)_{32}$ were dissolved in MeCN at room temperature) showed the presence of additional species that were not sufficiently abundant to be apparent in the ^{1}H NMR spectrum. The strong series of peaks corresponding to the series $\{Cd_{16}L_{24}(BF_4)_{32-n}\}^{n+}$ has almost disappeared and been replaced by several new peaks which can be separated into series corresponding to the octanuclear species $\{Cd_8L_{12}(BF_4)_{16-n}\}^{n+}$ (at m/z 2247, 1662, and 1313 for n = 3−5), the hexanuclear species $\{Cd_6L_9(BF_4)_{12-n}\}^{n+}$ (at m/z 1225 and 963 for n = 4 and 5), and the tetranuclear species $\{Cd_4L_6(BF_4)_{8-n}\}^{n+}$ (at m/z 3412, 1662, 1079, 788, and 613 for n = 1−5). Numerous smaller fragmentation products were also present at lower m/z values. The identity of these could be clearly confirmed from the isotope spacings, even when several peaks overlap at the same m/z value; for example, expansion of the isotope cluster at m/z 1662 clearly confirms the presence of three distinct species with charges of +1, +2, and +4, ascribed to $\{Cd_2L_3(BF_4)_3\}^+$, $\{Cd_4L_6(BF_4)_6\}^{2+}$, and $\{Cd_8L_{12}(BF_4)_{12}\}^{4+}$ (Figure 13). Importantly each ion series for a specific polynuclear fragment has at least one member that is unique and

dx.doi.org/10.1021/ja107403p | J. Am. Chem. Soc. 2011, 133, 858–870

cannot arise from a different cluster with a different charge; for example, the peaks at m/z 1313, 963, and 613, all of which have isotope spacings of 0.2 unit, can arise *only* from $\{Cd_8L_{12}(BF_4)_{11}\}^{5+}$, $\{Cd_6L_9(BF_4)_7\}^{5+}$, and $\{Cd_4L_6(BF_4)_3\}^{5+}$, respectively.

Clearly, therefore, the intensity of signals in the ES mass spectrum is not a reliable guide in this instance to relative abundances in solution. While the ES mass spectrum reveals the presence of Cd_8L_{12}, Cd_6L_9, and Cd_4L_6 cages after rearrangement of the starting $Cd_{16}L_{24}$ cage, the ^{1}H NMR spectrum shows completely unambiguously that the Cd_6L_9 trigonal prism is the principal product, with the other products being very minor species that are present only at levels that are not detectable by NMR spectroscopy.

We conclude therefore that $[Cd_{16}L_{24}](BF_4)_{32}$ is a kinetic product formed only on crystallization, but it rearranges in solution (on a time scale of weeks at room temperature but hours at 60 °C) to give principally $[Cd_6L_9](BF_4)_{12}$, whose structure is similar to that of the Cu(II) complex described above. It may be significant that both of these structures are based on different combinations of triangular Cd_3L_3 panels (cf. Figure 8), such that rearrangement of the larger cage into the smaller one can proceed via partial dissociation through intermediates in which the Cd_3L_3 panels are conserved but end up being recombined in different ways.

Metal/Ligand Assembly Experiments in Solution Followed by Mass Spectrometry. A similar picture was obtained by doing this experiment in reverse, that is, combining $Cd(BF_4)_2$ with L in a 2:3 ratio in CD_3CN and following the evolution of the ^{1}H NMR spectrum and the ES mass spectrum. Within 30 min of mixing the components, the ^{1}H NMR spectrum, albeit rather messy, clearly shows that the main product of the assembly is $[Cd_6L_9](BF_4)_{12}$ [compare Figure 11d, which shows part of the ^{1}H NMR spectrum of the $Cd(BF_4)_2$/L mixture in CD_3CN, with Figure 11c, which shows formation of the Cd_6L_9 cage at the end of the rearrangement of the $Cd_{16}L_{24}$ cage]. This spectrum does not change significantly over a period of days, indicating that when the metal salt and ligand are combined, the mixture reaches equilibrium rapidly (within 30 min), with the Cd_6L_9 cage being the most abundant product, and that the $Cd_{16}L_{24}$ cage is present only in small amounts.

A similar picture emerges from the ES mass spectral studies. The mass spectrum taken 30 min after mixing is dominated by numerous small fragments such as CdL_2, CdL_3, Cd_2L_2, Cd_2L_3, and so on, each associated with varying numbers of anions. At higher m/z values there are, however, a few weak peaks such as m/z 1312 for $\{Cd_8L_{12}(BF_4)_{11}\}^{5+}$, 1225 for $\{Cd_6L_9(BF_4)_8\}^{4+}$, and 1080 for $\{Cd_4L_6(BF_4)_5\}^{3+}$, with the last of these being the most intense (although, as noted above, intensity in the mass spectrum is not a reliable guide to abundance, and the NMR spectrum clearly shows the Cd_6L_9 cage to be the most abundant). So Cd_4, Cd_6,and Cd_8 cages do start to form within half an hour; but there is no sign of the expected sequence of peaks for the Cd_{16} cage. After 1 month the only significant difference is that the peaks for the low-nuclearity fragments have declined in significance, and the most intense sequence of product peaks corresponds to tetranuclear $\{Cd_4L_6(BF_4)_{8-n}\}^{n+}$ (n = 2−5) with weaker peaks present for $\{Cd_6L_9(BF_4)_{12-n}\}^{n+}$ (n = 4) and $\{Cd_8L_{12}(BF_4)_{16-n}\}^{n+}$ (n = 3−5). The series of peaks that we obtained for the intact cage $\{Cd_{16}L_{24}(BF_4)_{24-n}\}^{n+}$ following dissolution of the crystals is notable by its absence.

The conclusion, therefore, is the same as that which was reached from the disassembly experiment above: the Cd_{16} cage $[Cd_{16}L_{24}](BF_4)_{32}$ is the kinetic crystallization product, but in solution a mixture of smaller cages forms, of which (on the basis of NMR spectra) the trigonal prismatic $[Cd_6L_9](BF_4)_{12}$ complex is the most abundant. Conversion of the Cd_{16} cage to the Cd_6 cage in solution can be simply understood from the basic principles of equilibria. All other things being equal (e.g., no significant enthaplic change in the sum of the Cd−N bond strengths following the rearrangement), the higher abundance of the smaller Cd_6 cage in solution compared to the Cd_{16} cage is understandable on purely entropic grounds, which will favor formation of a larger number of smaller assemblies. If we assume an equilibrium involving only the two fully assembled cages (eq 1)

$$Cd_{16}\text{cage} = 2.67(Cd_6\text{cage}) \quad (1)$$

$$[Cd_{16}\text{cage}] = K[Cd_6\text{cage}]^{2.67} \quad (2)$$

the associated equilibrium constant (eq 2) implies that as the concentration increases, the balance quickly shifts away from the Cd_6 cage to the Cd_{16} cage: every factor of 10 increase in the concentration of Cd_6 requires an increase of the Cd_{16} concentration by an *additional* factor of 468 ($10^{2.67}$) to maintain the equilibrium constant. Thus, a shift in concentration domain from millimolar (solution) to molar (solid state) will favor the larger cage by a factor of 10^8, which is enough to give a complete switch from >99.99% of the smaller cage (solution) to >99.99% of the larger cage (solid).

A similar mixture of species is obtained both from slow *disassembly* of the $Cd_{16}L_{24}$ cage (weeks at room temperature) and from the more rapid *assembly* of the $Cd(BF_4)_2$/L mixture in a 2:3 ratio (minutes). The slowness with which $[Cd_{16}L_{24}](BF_4)_{32}$ dissociates and rearranges is testament to the kinetic stability imparted by the mutually intertwined and stacked array of ligands[18], which prevents the ligand dissociation that must be the first step.

The assembly experiment involving $Cu(BF_4)_2$ and L in a 2:3 ratio in MeCN was straightforward. Within a few minutes of preparing the mixture, the ES mass spectrum showed a strong sequence of peaks at m/z 1565, 1152, 904, 739, and 621 corresponding to the series $\{Cu_6L_9(BF_4)_{12-n}\}^{n+}$ (n = 3−7); the only other peaks of significance corresponded to mononuclear and dinuclear fragments, with no evidence for any higher nuclearity cages. This spectrum had hardly changed 2 days later, indicating that the trigonal prismatic hexanuclear cage is the most stable assembly involving Cu(II) and L in this ratio and that it forms in minutes; this is all consistent with what we saw in the ES mass spectrum of redissolved crystals of $[Cu_6L_9](BF_4)_{12}$.

Finally, we followed the reaction of $Ni(BF_4)_2$ and L in a 2:3 ratio in MeCN solution in the same way. The ES mass spectrum 2 min after preparation of the mixture was very complicated and could not be completely assigned, but we could identify peaks corresponding to a wide range of species including Ni_2L_3, Ni_2L_4, Ni_3L_4, Ni_3L_5, Ni_4L_6, and Ni_6L_9 clusters, each associated with varying numbers of counterions. We could not identify any clear peaks for the octanuclear Ni_8L_{12} cube at this stage. The spectrum steadily simplified with time, however, and after 2 weeks was dominated by a series of peaks at m/z 1555, 1144, 898, 734, and 617, corresponding to the hexanuclear species $\{Ni_6L_9(BF_4)_{12-n}\}^{n+}$ (n = 3−7). Significantly, the species with charges of 5+ and 7+ are unique to this series and cannot arise from any other simple metal/ligand/anion combination; as before, the charges were

Table 1. Crystal Parameters, Data Collection, and Refinement Details for the Structures in This Paper

complex	$[Cd_{16}L_{24}](ClO_4)_{32}\cdot 23MeCN$	$[Zn_{16}L_{24}](BF_4)_{32}\cdot 6MeCN\cdot 11H_2O$	$[Ni_8L_{16}](BF_4)_{12}(SiF_6)_2\cdot 18MeNO_2$	$[Cu_6L_9](BF_4)_{12}$
formula	$C_{622}H_{549}Cd_{16}Cl_{32}N_{167}O_{128}$	$C_{588}H_{520}B_{32}F_{128}N_{150}O_{11}Zn_{16}$	$C_{306}H_{294}B_{12}O_{36}Si_2N_{90}F_{60}Ni_8$	$C_{216}H_{180}B_{12}Cu_6F_{48}N_{54}$
formula weight	15 344.31	13 687.59	7603.89	4955.10
T, K	100(2)	100(2)	120(2)	150(2)
λ, Å	1.541 78	1.541 78	0.710 73	0.710 73
crystal system	triclinic	monoclinic	hexagonal	orthorhombic
space group	*P*-1	*C*2/*c*	*R*-3*c*	*Iba*2
a, Å	29.7224(8)	31.117(3)	26.0607(3)	31.7261(11)
b, Å	30.1896(8)	51.828(3)	26.0607(3)	56.9758(17)
c, Å	52.4872(13)	48.797(3)	98.7782(14)	29.7638(9)
α, deg	87.5810(10)	90	90	90
β, deg	79.9780(10)	99.950(2)	90	90
γ, deg	70.1050(10)	90	120	90
V, Å^3	43 603(2)	77 513(9)	58 098.3(13)	53 802(3)
Z	2	4	6	8
D_{calc}, Mg/m^3	1.138	1.173	1.300	1.095
μ, mm^{-1}	4.394	1.281	0.485	0.535
F(000)	15 180	27 912	23 340	18 192
crystal size, mm	0.25 × 0.2 × 0.1	0.3 × 0.2 × 0.2	0.2 × 0.2 × 0.1	0.3 × 0.3 × 0.2
independent data	118 370 [R(int) = 0.0501]	67 955 [R(int) = 0.1181]	14 798 [R(int) = 0.0494]	54 501 [R(int) = 0.1517]
restraints	41 577	3443	13	2673
parameters	3875	1734	652	2071
*R*1, w*R*2	0.127, 0.382	0.188, 0.470	0.129, 0.410	0.107, 0.323

confirmed by isotopic spacings. A much weaker series of peaks could be seen at m/z 1227, 1008, and 851 corresponding to the (expected) cubelike octanuclear species $\{Ni_8L_{12}(BF_4)_{16-n}\}^{n+}$ (n = 5−7). This again is consistent with what we observed in the mass spectrum of redissolved crystals of the octanuclear cube: the cube persists in solution but the hexanuclear trigonal prismatic species is also present, with the larger cube being a minor product that is favored during crystallization for the same reasons as apply to the Cd_{16} cage.

CONCLUSIONS

The simple bis-bidentate bridging ligand L combines with six-coordinate transition metal dications to afford cage complexes all having a 2M:3 L ratio, which results in a polyhedral cage, with a metal ion at each vertex (3-connected) and a bridging ligand spanning each edge (2-connected). This simple stoichiometric principle is expressed in a surprising variety of structures in the solid state: the Ni(II) complex is an octanuclear Ni_8L_{12} cube; the Cu(II) complex is a hexanuclear Cu_6L_9 trigonal prism; and the Zn(II) and Cd(II) complexes are hexadecanuclear $M_{16}L_{24}$ cages that can be described as tetracapped truncated tetrahedra. These variations may be ascribed to differences in ionic radii and stereoelectronic preferences, especially the Jahn−Teller effect for Cu(II), which results in significantly distorted tris-chelate coordination geometries. The Ni_8L_{12} cube is of a structural type that we have seen before, but the Cu_6L_9 and $M_{16}L_{24}$ (M = Zn, Cd) cages are both new members of the set, with the $M_{16}L_{24}$ cages being the largest we have seen in this series: their assembly required 96 metal−ligand bonds to form with correct control of optical configuration at 16 metal centers. Both M_6L_9 and $M_{16}L_{24}$ structures consist of conserved triangular helical M_3L_3 panels that are interconnected in different ways.

NMR and ES mass spectrometric solution studies reveal complex solution behavior. The trigonal prismatic Cu_6L_9 forms quickly (minutes) when the metal ions and ligand are combined in the correct ratio and shows no evidence for rearrangement to other cages; thus, the crystal structure is also the thermodynamic product and is retained in solution. In contrast, redissolved crystals of the Ni_8L_{12} cube show that in solution a Ni_6L_9 assembly (presumably a trigonal prismatic cage) is also formed; the same result is obtained by combining Ni(II) salts and L in the correct ratio and allowing the solution to reach equilibrium.

The $Zn_{16}L_{24}$ and $Cd_{16}L_{24}$ cages do not persist in solution. The $Cd_{16}L_{24}$ cage was studied in detail and rearranges slowly, over a period of weeks at room temperature, to a mixture containing Cd_4L_6, Cd_6L_9, and Cd_8L_{12} cages, which presumably have tetrahedral, trigonal prismatic, and cubic structures, respectively. Of these, the Cd_6L_9 trigonal prismatic cage is by far the most abundant and dominates the ^{1}H NMR spectrum. The $Cd_{16}L_{24}$ tetracapped truncated tetrahedral cage is therefore a crystallization product that dominates at high concentrations and slowly rearranges to the Cd_6L_9 trigonal prismatic cage in dilute solution; conversely, the Cd_6L_9 complex forms in minutes after $Cd(BF_4)_2$ is mixed with L in the correct proportion.

EXPERIMENTAL SECTION

General Details. The ligand L was prepared as described previously,[4] as were complexes $[Zn_{16}L_{24}]X_{32}$ and $[Cd_{16}L_{24}]X_{32}$ (X = perchlorate or tetrafluoroborate), which were briefly described in a preliminary communication.[4] Electrospray (ES) mass spectra were recorded on a Micromass LCT instrument at a low cone voltage (typically 5 V) for solutions of the complexes in MeCN. ^{1}H and ^{113}Cd NMR spectra were recorded on Bruker DRX-500 or Avance-2 400 instruments, respectively.

Preparation of $[Cu_6L_9](BF_4)_{12}$. A solution of $Cu(BF_4)_2$ (0.023 g, 0.1 mmol) in MeOH (7 cm^3) was added to a solution of L (0.058 g, 0.15 mmol) in CH_2Cl_2 (7 cm^3). The mixture was stirred at room

dx.doi.org/10.1021/ja107403p |J. Am. Chem. Soc. 2011, 133, 858–870

temperature for 24 h, and the resultant precipitate was filtered off, washed with both MeOH and CH_2Cl_2, and dried in vacuo to give $[Cu_6L_9](BF_4)_{12}$ as a green powder in 80% yield. X-ray-quality crystals were grown by slow diffusion of isopropyl ether into a solution of the complex in acetonitrile or nitromethane. ES-MS data: see main text. Elemental analytical data of vacuum-dried samples were consistent with the presence of water of crystallization due to the desolvated material being hygroscopic, as follows. Found: C, 50.2%; H, 3.6%; N, 14.3%. Required for $[Cu_6L_9](BF_4)_{12}\cdot 10H_2O$: C, 50.5%; H. 3.9%; N, 14.7%.

Preparation of $[Ni_8L_{12}](BF_4)_{16}$. A Teflon-lined autoclave was charged with $Ni(BF_4)_2$ (0.085 mmol, 0.029 g), L (0.13 mmol, 0.050 g), and methanol (9 cm^3). The mixture was heated to 100 °C for 12 h and then cooled slowly at 0.1 °C·min^{-1} to room temperature to yield a microcrystalline product that was further recrystallized from $MeNO_2$/diethyl ether. The crystal used for the structural analysis was found to contain hexafluorosilicate anions as well as tetrafluoroborate (see main text). Elemental analytical data of vacuum-dried samples were consistent with the presence of water of crystallization due to the desolvated material being hygroscopic, as follows. Found: C, 50.2%; H, 3.8%; N, 14.6%. Required for $[Ni_8L_{12}](BF_4)_{16}\cdot 15H_2O$: C, 50.6%; H, 4.0%; N, 14.7%.

As mentioned in the main text, we cannot rule out the possibility that some Ni_6L_9 species is also formed in the solid state (cf. the ES mass spectral data); this would of course have the same elemental analytical data. Attempts to determine phase purity of the crystalline material by powder diffraction were unsuccessful, as rapid solvent loss from the crystals generated amorphous material with no Bragg reflections.

X-ray Crystallography. Crystals were removed from the mother liquor, coated with oil, and transferred to a stream of cold N_2 on the diffractometer as quickly as possible to prevent decomposition due to solvent loss. The structures of $[Cd_{16}L_{24}](ClO_4)_{32}$ and $[Zn_{16}L_{24}](BF_4)_{32}$ were determined at the University of Bristol on a Bruker Proteum diffractometer equipped with Cu Kα radiation from a rotating anode generator; the structure of $[Cu_6L_9](BF_4)_{12}$ was determined at the University of Sheffield on a Bruker APEX-2 diffractometer equipped with Mo Kα radiation from a sealed-tube source; and the structure of $[Ni_8L_{12}](BF_4)_{12}(SiF_6)_2$ was determined at the EPSRC National Crystallography Service at the University of Southampton, on a Nonius Kappa-CCD diffractometer equipped with Mo Kα radiation from a Bruker-Nonius FR-591 rotating anode generator. Details of the crystal parameters, data collection, and refinement are summarized in Table 1.

As usual for cage complexes of this nature, crystals of the metal complexes scattered weakly due to the extensive disorder of anions and solvent molecules. After integration of the raw data and before merging, an empirical absorption correction was applied (SADABS),[19] based on comparison of multiple symmetry-equivalent measurements. The structures were solved by direct methods and refined by full-matrix least-squares on weighted F^2 values for all reflections by use of the SHELX suite of programs.[20] Pertinent crystallographic data are collected in Table 1. In every case (i) the weakness of the data required extensive use of restraints and/or constraints, to keep the geometries of anions, aromatic rings, or solvent molecules reasonable; and (ii) there was disordered associated with anions and (where located) solvent molecules. In addition, in all cases there were extensive areas of residual electron density that could not sensibly be modeled as solvent or anions, which were removed via application of the Squeeze function in PLATON.[21] Full details of these issues and how they were handled is given in the individual CIFs (Supporting Information).

■ ASSOCIATED CONTENT

Supporting Information. Crystallographic CIF files for the new structures. This material is available free of charge via the Internet at http://pubs.acs.org.

■ AUTHOR INFORMATION

Corresponding Author
m.d.ward@sheffield.ac.uk

■ ACKNOWLEDGMENT

We thank the EPSRC (U.K.) for financial support, Dr. John C. Jeffery (University of Bristol) and Mr. Harry Adams (University of Sheffield) for assistance with the X-ray crystallography, and Professor Chris Hunter for valuable discussions. We also thank the EPSRC National Crystallography Service for collecting the data used in the structural determination of $[Ni_8L_{12}](BF_4)_{12}(SiF_6)_2$.

■ REFERENCES

(1) Reviews on coordination cages: (a) Fiedler, D.; Leung, D. H.; Bergman, R. G.; Raymond, K. N. *Acc. Chem. Res.* **2005,** *38*, 349. (b) Fujita, M.; Tominaga, M.; Hori, A.; Therrien, B. *Acc. Chem. Res.* **2005,** *38*, 369. (c) Seidel, S. R.; Stang, P. J. *Acc. Chem. Res.* **2002,** *35*, 972. (d) Hamilton, T. D.; MacGillivray, L. R. *Cryst. Growth Des.* **2004,** *4*, 419. (e) Ward, M. D. *Chem. Commun.* **2009,** 4487. (f) Perry, J. J.; Perman, J. A.; Zaworotko, M. J. *Chem. Soc. Rev.* **2009,** *38*, 1400. (g) Alvarez, S. *Dalton Trans.* **2006,** 2209.

(2) Representative recent examples of coordination cages: (a) Sun, Q.-F.; Iwasa, J.; Ogawa, D.; Ishido, Y.; Sato, S.; Ozeki, T.; Sei., Y.; Yamaguchi, K.; Fujita, M. *Science* **2010,** *328*, 1144. (b) Wang, M.; Zheng, Y.-R.; Ghosh, K.; Stang, P. J. *J. Am. Chem. Soc.* **2010,** *132*, 9282. (c) Mal, P.; Schultz, D.; Beyeh, K.; Rissanen, K.; Nitschke, J. R. *Angew. Chem., Int. Ed.* **2008,** *47*, 8297. (d) Oppel, I. M.; Föcker, K. *Angew. Chem., Int. Ed.* **2008,** *47*, 402. (e) Brasey, T.; Scopelliti, R.; Severin, K. *Chem. Commun.* **2006,** 3308. (f) Al-Rasbi, N. K.; Tidmarsh, I. S.; Argent, S. P.; Adams, H.; Harding, L. P.; Ward, M. D. *J. Am. Chem. Soc.* **2008,** *130*, 11641. (g) Bar, A. K.; Chakrabarty, R.; Mukherjee, P. S. *Inorg. Chem.* **2009,** *48*, 10880. (h) Umakoshi, K.; Yamauchi, Y.; Nakamiya, K.; Kojima, T.; Yamasaki, M.; Kawano, H.; Onishi, M. *Inorg. Chem.* **2003,** *42*, 3907. (i) Yu, S.-Y.; Jiao, Q.; Li, S.-H.; Huang, H.-P.; Li, Y.-Z.; Pan, Y.-J.; Sei, Y.; Yamaguchi, K. *Org. Lett.* **2007,** *99*, 1379.

(3) Host−guest chemistry of coordination cages: (a) Yoshizawa, M.; Klosterman, J.; Fujita, M. *Angew. Chem., Int. Ed.* **2009,** *48*, 3418. (b) Pluth, M. D.; Bergman, R. G.; Raymond, K. N. *Acc. Chem. Res.* **2009,** *42*, 1650. (c) Mirtschin, S.; Krasniqi, E.; Scopelliti, R.; Severin, K. *Inorg. Chem.* **2008,** *47*, 6375. (d) Clever, G. H.; Tashiro, S.; Shionoya, M. *Angew. Chem., Int. Ed.* **2009,** *48*, 7010. (e) Custelcean, R.; Bosano, J.; Bonnesen, P. V.; Kertesz, V.; Hay, B. P. *Angew. Chem., Int. Ed.* **2009,** *48*, 4025.

(4) Argent, S. P.; Adams, H.; Riis-Johannessen, T.; Jeffery, J. C.; Harding, L. P.; Ward, M. D. *J. Am. Chem. Soc.* **2006,** *128*, 72.

(5) (a) Argent, S. P.; Adams, H.; Riis-Johannessen, T.; Jeffery, J. C.; Harding, L. P.; Mamula, O.; Ward, M. D. *Inorg. Chem.* **2006,** *45*, 3905. (b) Schweiger, M.; Yamamoto, T.; Stang, P. J.; Blaser, D.; Boese, R. *J. Org. Chem.* **2005,** *70*, 4861. (c) Müller, I. M.; Robson, R.; Separovic, R. *Angew. Chem., Int. Ed.* **2001,** *40*, 4385.

(6) Hunter, C. A.; Sanders, J. K. M. *J. Am. Chem. Soc.* **1990,** *112*, 5525. Claessens, C. G.; Stoddart, J. F. *J. Phys. Org. Chem.* **1997,** *10*, 254.

(7) Tidmarsh, I. S.; Faust, T. B.; Adams, H.; Harding., L. P.; Russo, L.; Clegg, W.; Ward, M. D. *J. Am. Chem. Soc.* **2008,** *130*, 15167.

(8) (a) Tidmarsh, I. S.; Taylor, B. F.; Hardie, M. J.; Russo, L.; Clegg, W.; Ward, M. D. *New J. Chem.* **2009,** *33*, 366. (b) Paul, R. L.; Bell, Z. R.; Jeffery, J. C.; McCleverty, J. A.; Ward, M. D. *Proc. Natl. Acad. Sci. U.S.A.* **2002,** *99*, 4883.

(9) Najar, A. M.; Tidmarsh, I. S.; Adams, H.; Ward, M. D. *Inorg. Chem.* **2009,** *48*, 11871.

(10) (a) Kuehl, C. J.; Kryschenko, Y. K.; Radhakrishnan, U.; Seidel, S. R.; Huang, S. D.; Stang, P. J. *Proc. Natl. Acad. Sci U.S.A.* **2002,** *99*, 4932. (b) Kuehl, C. J.; Yamamoto, T.; Seidel, S. R.; Stang, P. J. *Org. Lett.*

2002, *4*, 913. (c) Zheng, Y.-R.; Yang, H.-B.; Ghosh, K.; Zhao, L.; Stang, P. *Chem.—Eur. J.* **2009,** *15*, 7203.

(11) (a) Su, C.-Y.; Cai, Y.-P.; Chen, C.- L.; Lissner, F.; Kang, B. S.; Kaim, W. *Angew. Chem., Int. Ed.* **2002,** *41*, 3371. (b) Su, C.-Y.; Cai, Y.-P.; Chen, C.-L.; Smith, M. D.; Kaim, W.; zur Loye, H.-C. *J. Am. Chem. Soc.* **2003,** *125*, 8595.

(12) Ghosh, S.; Mukherjee, P. S. *Organometallics* **2008,** *27*, 316.

(13) Contakes, S. M.; Rauchfuss, T. B. *Angew. Chem., Int. Ed.* **2000,** *39*, 1984.

(14) Alternatively, one can use the Stokes—Einstein equation to estimate the hydrodynamic radius of a molecule from the diffusion coefficient: this gives radii of 15.9 Å for the Cd_{16} complex and 11.4 Å for the Cd_6 complex. These values are likely to be smaller than the "real" radius if the molecules are nonspherical, which is the case here. For the Cd_{16} complex the distance from the center to the most remote H atom is 18 Å, but at other points the "radius" is less than this. For the trigonal prismatic Cd_6 complex, which is more anisotropic in shape, the maximum "radius" is about 12 Å (based on the Cu_6 structure). Thus the hydrodynamic radii estimated from the diffusion coefficients are fully consistent with the observed structures.

(15) (a) Paul, R. L.; Bell, Z. R.; Jeffery, J. C.; McCleverty, J. A.; Ward, M. D. *Proc. Natl. Acad. Sci. U.S.A.* **2002,** *99*, 4883. (b) Tidmarsh, I. S.; Taylor, B. F.; Hardie, M. J.; Russo, L.; Clegg, W.; Ward, M. D. *New J. Chem.* **2009,** *33*, 366.

(16) Paul, R. L.; Argent, S. P.; Jeffery, J. C.; Harding, L. P.; Lynam, J. M.; Ward, M. D. *Dalton Trans.* **2004,** 3453.

(17) After more than about 2 days at 60 °C, the NMR sample decomposed with the appearance of a white precipitate. This contained traces of free ligand (by ES-MS) and some insoluble material, which we assume to be Cd(II)—fluoride complexes, given the ease with which the $[BF_4]^-$ anion can decompose. See for example: Fenton, H.; Tidmarsh, I. S.; Ward, M. D. *Dalton Trans.* **2009,** 4199.

(18) (a) Davis, A. V.; Yeh, R. M.; Raymond, K. N. *Proc. Natl. Acad. Sci. U.S.A.* **2002,** *99*, 4793. (b) Terpin, A. J.; Ziegler, M.; Johnson, D. W.; Raymond, K. N. *Angew. Chem., Int. Ed.* **2001,** *40*, 157.

(19) Sheldrick, G. M. *SADABS: A program for absorption correction with the Siemens SMART system*; University of Gottingen, Germany, 1996.

(20) Sheldrick, G. M. *Acta Crystallogr., Sect. A* **2008,** *64*, 112.

(21) Spek, A. L. *J. Appl. Crystallogr.* **2003,** *36*, 7.